

Combining sequential extractions with bulk and micro X-ray spectroscopy to elucidate iron and phosphorus speciation in sediments of an iron-treated peat lake

Melanie A. Münch, Andreas Voegelin, Luis Carlos Colocco Hurtarte, Jörg Göttlicher, Thilo Behrends

Royal Society of Chemistry – Environmental Science: Processes & Impacts, 2024

DOI: [10.1039/D4EM00402G](https://doi.org/10.1039/D4EM00402G)

Electronic supplementary information

A – Sample information

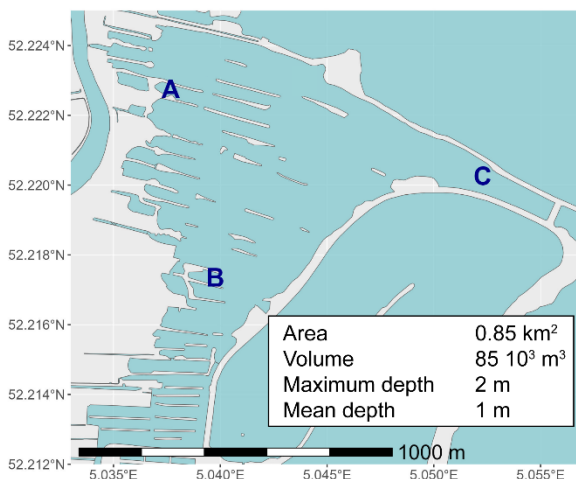


Figure A1: Lake Terra Nova in the Netherlands with lake property information and the three coring sites (A-C). (Adapted from (Münch et al., 2023)).

The criteria for sampling site selection, the sediment samples and their chemical analysis used in this study are described in detail in (Münch et al., 2023). For all the depth-resolved sediment analysis, one core from stations A, B and C each were used. Total elemental content, sequential extraction and porewater analysis were performed on cores A, B and C. Depth profiles displaying averages represent the averaged data from the three cores A, B and C. Correlations of data from chemical analysis were calculated using data from all three cores.

As illustrated in Figure 1 of the main paper, the three sediment cores are comparable when it comes to total elemental content. Due to availability of sample material, sediment from two different cores were used for the XAS measurements. Cores from sites A and B were selected for XAS measurements since the sedimentation regime at these two sites is comparable to each other, as opposed to site C (Münch et al., 2023). Depth-resolved bulk-XAS measurements were performed on core B, the focused-beam XAS measurements were performed on core A. Correlations of data gained by chemical analysis and XAS were calculated using only data from the core the XAS measurements were done on.

B – Fe K-edge XAS

B1 – Fe K-edge reference spectra

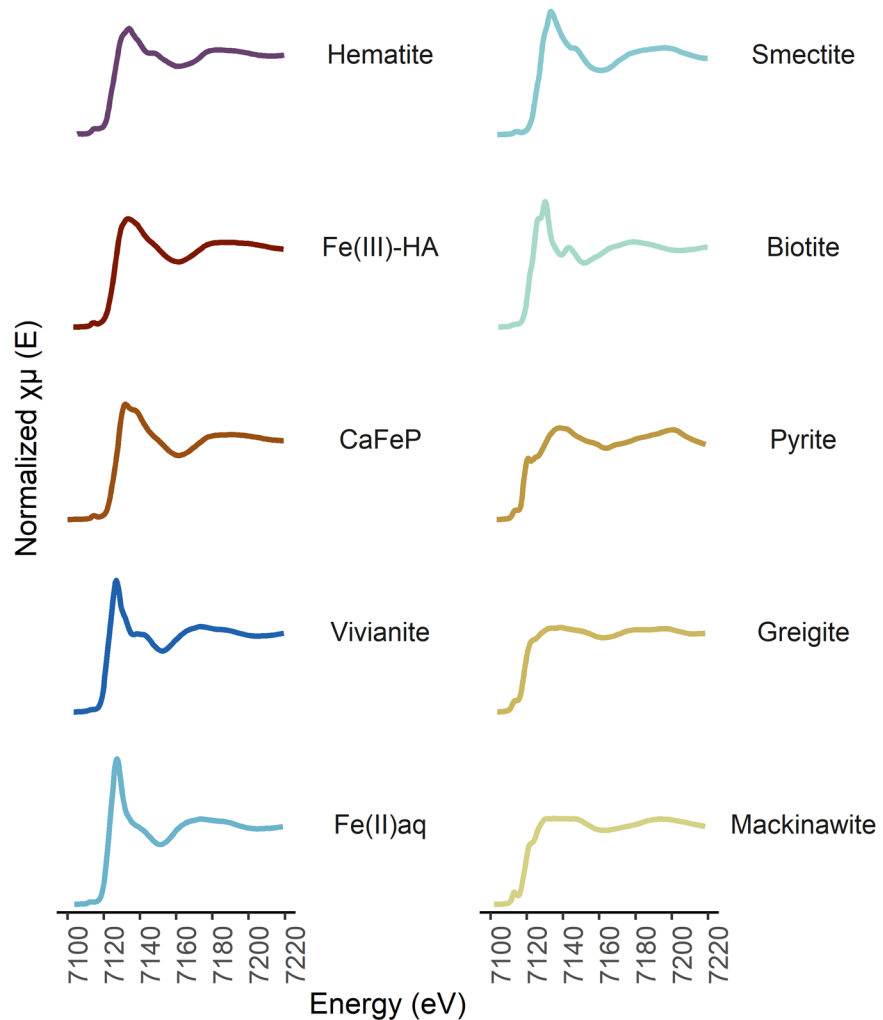


Figure B1-1: Reference spectra used for linear combination fitting of the collected Fe K-edge μ -XANES spectra.

B2 – Fe K-edge bulk XAS spectra

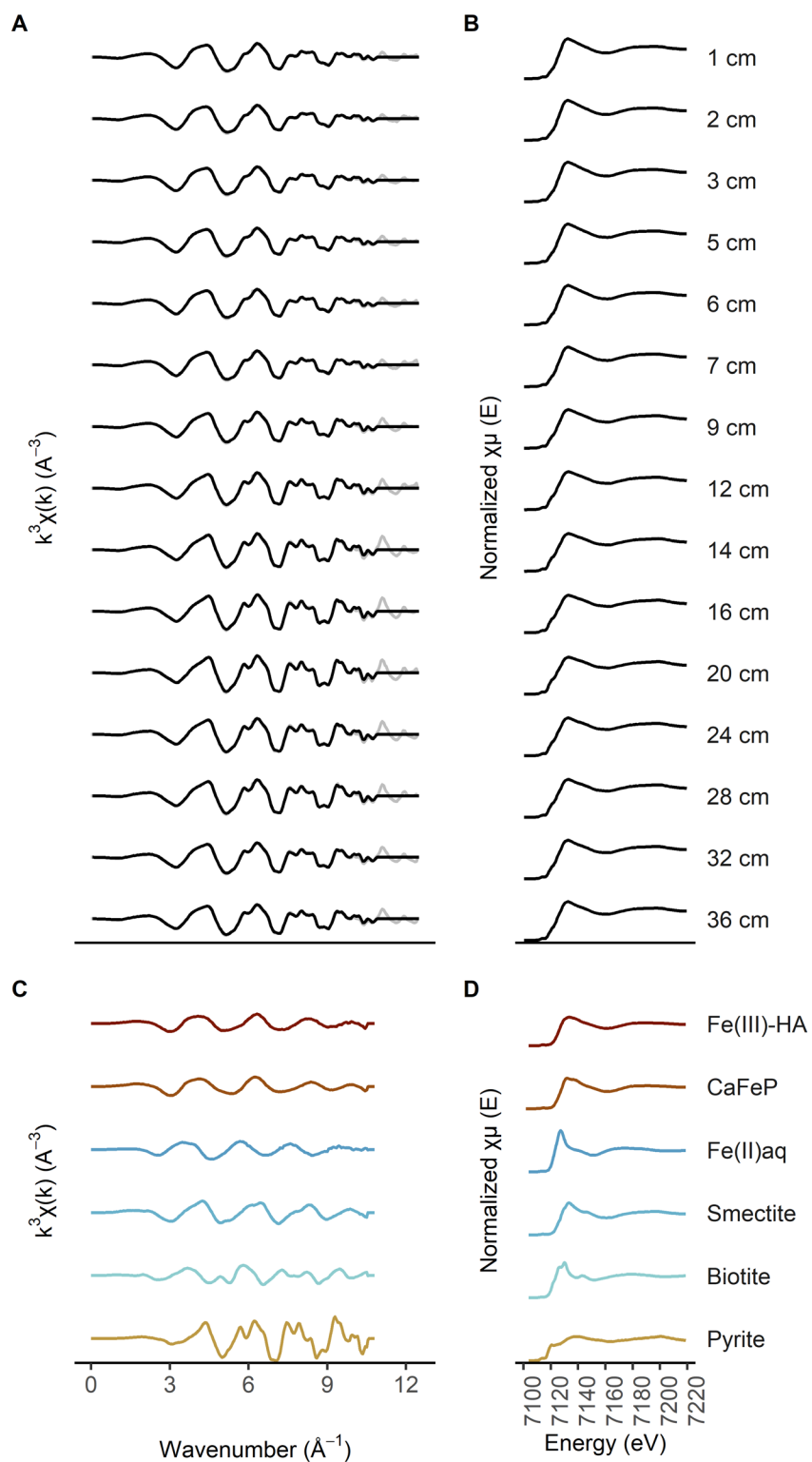


Figure B2-1: Depth-resolved bulk Fe K-edge EXAFS (A) and XANES (B) spectra (grey) and linear combination fits (black). EXAFS (C) and XANES (D) spectra of the references used for linear combination fits. Details on the references are available in ESI Table B1-1. The LCF data is available in ESI Tables B3-1 and -2.

B4 – Fe K-edge μ -XANES LCF data

Table B4-1: LCF results for the average Fe μ -XANES spectra collected on two sediment samples from 2 and 40 cm depth in fractions of total Fe. The results are shown normalized to a sum of unity, together with the effective sum of the fitted fractions.

Depth (cm)	Average spectrum		XANES LCF											
			fitted sum	r-factor	Fe(III)-HA	Fe(II)aq	CaFeP	Smectite	Biotite	Pyrite	Greigite	Mackinawite	Hematite	Vivianite
2	Type 1	t-T1-Fe	1.01	9 E-4	—	0.20	0.14	0.25	0.15	0.26	—	—	—	—
	Type 2	t-T2-Fe	1.00	1 E-3	—	0.06	0.00	—	0.05	0.88	—	—	—	—
	Type 3	t-T3-Fe	1.01	7 E-4	—	0.13	0.07	0.18	0.13	0.50	—	—	—	—
	Region 1	t-R1-Fe	1.02	2 E-2	—	0.20	—	—	0.36	—	0.44	—	—	—
	Region 2	t-R2-Fe	1.01	2 E-3	—	0.09	—	0.06	—	0.46	0.39	—	—	—
	Region 3	t-R3-Fe	1.01	4 E-3	—	—	—	0.11	0.17	—	0.51	—	—	0.21
	Region 4	t-R4-Fe	1.01	2 E-3	—	—	0.10	—	—	0.26	—	0.41	—	0.23
40	Type 1	b-T1-Fe	1.01	8 E-4	—	0.14	0.07	0.32	0.26	0.21	—	—	—	—
	Type 2	b-T2-Fe	1.01	7 E-4	—	0.12	—	0.22	—	0.43	0.23	—	—	—
	Type 3	b-T3-Fe	1.01	9 E-4	—	0.13	0.05	0.22	0.18	0.41	—	—	—	—
	Type 4	b-T4-Fe	1.01	9 E-4	—	0.04	—	0.02	0.09	0.85	—	—	—	—
	Region 1	b-R1-Fe	1.01	2 E-3	—	—	—	0.33	0.33	—	0.15	—	—	0.19
	Region 2	b-R2-Fe	1.01	1 E-3	—	0.11	—	0.28	0.51	0.10	—	—	—	—
	Region 3	b-R3-Fe	1.00	3 E-3	0.13	—	—	—	—	—	0.65	0.19	—	0.03
	Region 4	b-R4-Fe	1.00	-	—	—	—	—	—	1	—	—	—	—
	Region 5	b-R5-Fe	1.01	3 E-3	—	0.11	—	—	—	0.09	—	—	0.81	—
	Region 6	b-R6-Fe	1.01	1 E-3	—	0.13	—	0.44	—	—	0.27	—	0.17	—
	Region 7	b-R7-Fe	1.01	2 E-3	—	0.20	0.18	0.10	0.06	0.47	—	—	—	—
	Region 8	b-R8-Fe	1.01	2 E-3	—	0.15	0.06	0.14	0.26	0.39	—	—	—	—
	Spot 1	b-S1-Fe	1.00	-	—	—	—	—	—	—	—	1	—	—

C – P K-edge XAS

C1 – P K-edge reference spectra

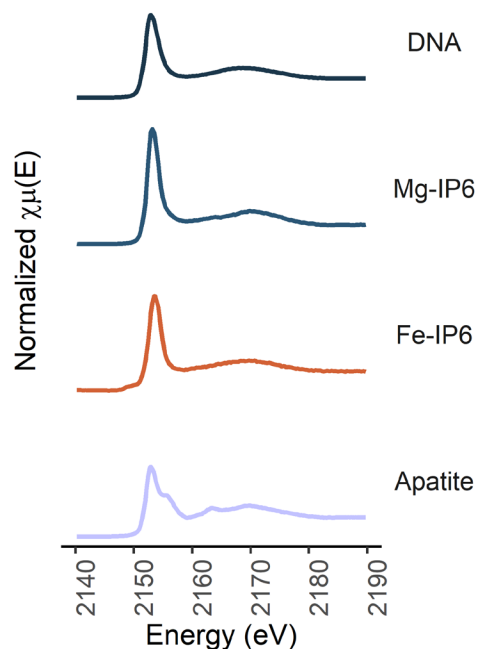


Figure C1-1: Reference P K-edge XANES spectra (details in ESI Table C1-1).

C2 – P K-edge bulk XANES spectra

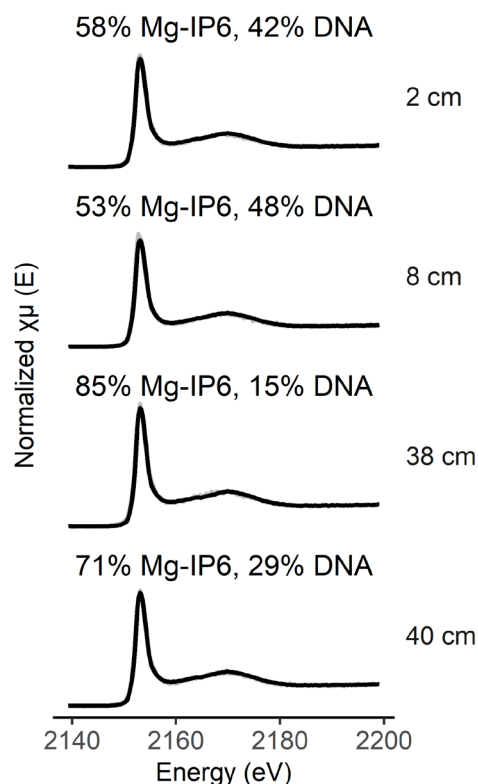


Figure C2-1: Depth-resolved bulk P K-edge XANES spectra (grey) and linear combination fits (black) with contribution of P references according to LCF annotated for each spectrum.

C3 – P K-edge bulk XANES LCF data

Table C3-1: LCF results of the bulk XANES spectra of samples from specific depth in fractions of total P. The results are shown normalized to sum one with the initial sum indicated in the respective column.

Depth (cm)	XANES LCF					
	fitted sum	r-factor	DNA	Mg-IP6	Fe-IP6	Apatite
2	1.00	1 E-3	0.42	0.58	—	—
8	1.00	3 E-3	0.48	0.53	—	—
38	1.00	2 E-3	0.15	0.85	—	—
40	1.00	8 E-4	0.29	0.71	—	—

C4 – P K-edge μ -XANES LCF data

Table C4-1: LCF results of the average P μ -XANES spectra collected on two samples from 2 and 40 cm depth in fractions of total P. The results are shown normalized to sum one with the initial sum indicated in the respective column.

Depth (cm)	Average spectrum		XANES LCF					
			fitted sum	r-factor	DNA	Mg-IP6	Fe-IP6	Apatite
2	Type 1	t-T1-P	1.00	6 E-4	0.40	0.53	—	0.06
	Spot 1	t-S1-P	1.00	2 E-3	0.15	0.10	0.53	0.23
	Spot 2	t-S2-P	1.00	2 E-3	—	—	—	1.00
40	Type 1	b-T1-P	1.00	1 E-3	0.32	0.66	0.02	—
	Type 2	b-T2-P	1.00	5 E-3	—	—	—	1.00
	Region 1	b-R1-P	1.00	2 E-3	0.12	0.39	0.14	0.35

D – spatially resolved micro-focused X-ray fluorescence (XRF) and XAS analysis

D1 – Photon flux induced beam damage

The first μ -XANES spectra that were collected using the focused beam at ID21 at ESRF were collected as 4 repeats to test for beam damage. Indeed, the 4 spectra collected on point of interest (poi) 31198 (dwell time 0.1s) show clear alteration of the sample material due to the irradiation, in this case the oxidation of Fe(II) in pyrite to Fe(III) (Figure D1-1). The beam damage starts with the second scan, but only becomes pronounced with the third scan. Due to this observation, the measurement strategy was changed to single spectra at many points instead of repeats.

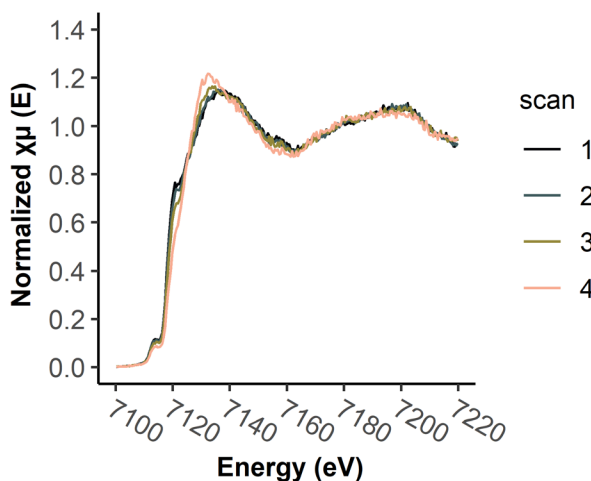


Figure D1-1: Repeat μ -XANES spectra measured on poi 31189 indicating beam damage in form or oxidation of Fe(II) in pyrite to Fe(III). Beam damage is most pronounced beginning with the 3rd scan.

Nevertheless, the sequence of first mapping the sample surface and then measuring point spectra probably caused some alteration to the sample material, most notably to the highly amorphous, low density Fe(III) phases associated to organic matter. Photoreduction of Fe(III) to Fe(II) coupled to oxidation of organic ligands is a well-known phenomenon (Abrahamson et al., 1994; Krizek et al., 1982;

Terzano et al., 2013) and its likelihood increases with increasing brilliance of synchrotron radiation beamlines (Bras et al., 2021).

In our samples, LCF of the XAS spectra systematically indicated more Fe(III) in the bulk phase than when measured spatially resolved with the focused beam as μ -XANES. To exclude beamline effects, the results of the different XAS measurements of the sediment sample from 2 cm depths were compared. The bulk XANES spectra measured at SUL-X (measured in transmission mode) and at ID21 (measured in fluorescence mode) were identical, once the ID21 measurement was self-absorption corrected (self-absorption of $\text{Fe(OH)}_3(\text{H}_2\text{O})_{160}$ with water content optimized to obtain a good pre-edge) (Figure D1-2A). According to LCF the bulk sediment consists of ca. 50% amorphous Fe(III) (Fe(III)-HA and CaFeP) (Figure D1-2B). As an approximation to a bulk phase measured by μ -XAS using the focused beam, the merged μ -XANES spectrum Type 1 (t-T1-Fe) was used, which represents the most abundant phase at 2 cm depth, with its individual spectra collected across the entire sample. The μ -XANES spectrum of Type 1 is similar in shape to the two bulk spectra, but with the edge-step slightly shifted to lower energies, indicating higher abundance of Fe(II) (Figure D1-2A). This is reflected in the LCF, which needed Fe(II)aq, considerably less CaFeP and no Fe(III)-HA for a good fit (Figure D1-2B).

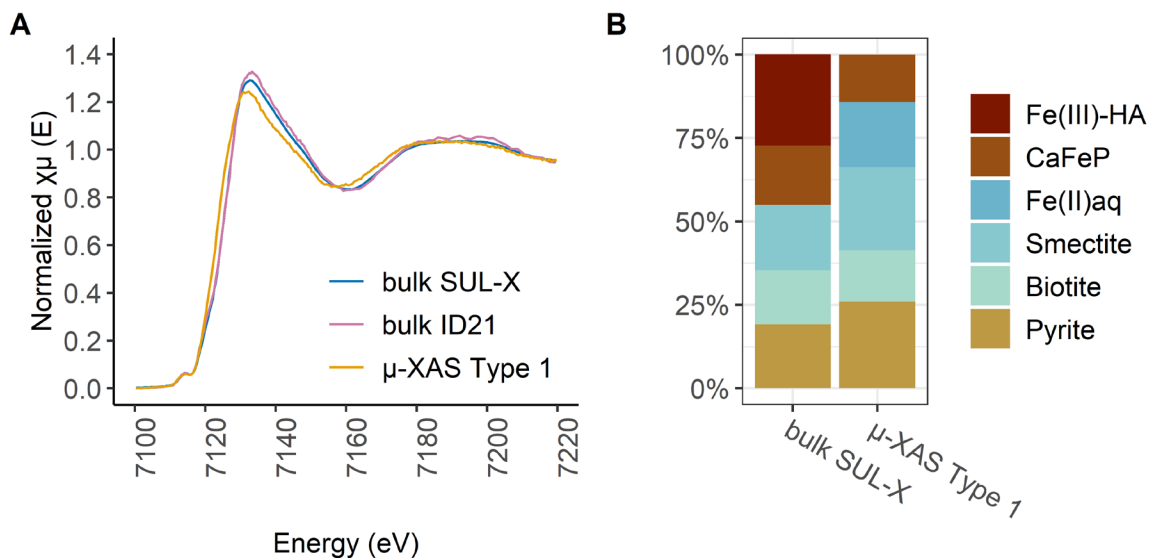


Figure D1-2: Comparison of XANES spectra collected on a bulk sample from 2 cm depth of core B at the SUL-X beamline at KIT (bulk SUL-X), a sample from 2 cm depth of core A collected at the ID21 beamline at ESRF in unfocused mode (bulk ID21) and in focused mode (μ -XAS Type 1) (A). The μ -XAS spectrum represents the most abundant phase based on comparison of all the μ -XAS spectra collected on this sample. Results of linear combination fitting of all three spectra show an overall shift towards Fe(II) in the spectra recorded in focused mode (B).

D2 – Identity of the μ -XANES spectra and μ -XRF maps

Table D2-1: Identity of the μ -XANES spectra (points of interest, poi). Spectra recorded at 2400 eV were collected in triplicates.

Element	Energy (eV)	top : 2 cm depth			bottom : 40 cm depth		
		Average spectrum	spectra ID (poi)	Found on μ XRF map (roi)	Average spectrum	spectra ID (poi)	Found on μ XRF map (roi)
Fe	7200	t-T1-Fe	31282, -84-90	31280	b-T1-Fe	31425-29	31419
			31303-04, -06-13	31302		31444	31375
			31316-26	31314		31471-75	31455
			31353, 31356-61	31340		31457-31501, -03, -06	31370
			31362-68	31189			
			31197	31220			
		t-T2-Fe	31213-14, -16		b-T2-Fe	31401-06	31396
			31198	31189		31446-47, -51-53	31375
			31233-42	31232		31456-57, -63-65, -68-70	31455
			31341-50	31339			
		t-T3-Fe	31209-10, -12	31220	b-T3-Fe	31445, -48-49	31375
			31305	31302		31461-62, -66-67	31455
			31354-55	31340			
			31364	31189			
P	2400	t-R1-Fe	31292-95, -97-31301	31291	b-T4-Fe	31397-31400	31396
						31450	31375
						31504	31370
			t-R2-Fe	31328		31433-38, -40-42	31432
		t-R3-Fe	31351-52	31340	b-R1-Fe	31409-11, -14-18	31408
			31333-34, -38	31328		31486, 88-90, 92, 94	31376
		t-R4-Fe			b-R2-Fe	31385-90	31381
						31420-24	31419
					b-R3-Fe	31458-60	31455
						31491, -93, -95	31376
					b-R7-Fe	31412-13	31408
						31487	31376
					t-T1-P	31539-42	31534
						31559-60	31556
S	2400	t-T1-P	31621-22	31620	t-T2-P	31565-66	31372
			31625-26	31624		31523-24	31512
			31627-30	31221		31552-53	31513
			31632, 34-35	31223		31557-58	31556
		t-S1-P	31631	31221	t-R1-P	31531-33	31529
S	2400	t-S2-P	31617	31189			

Table D2-2: Identity of the μ -XRF maps (region of interest, roi).

Element	Energy (eV)	top : 2 cm depth			bottom : 40 cm depth		
		Figure	μ XRF map ID (roi)	Resolution (μm)	Figure	μ XRF map ID (roi)	Resolution (μm)
Fe	7200	4A	31173_37784	10	4E	31369_37945	10
		4B, 4C	31223_37823	2	4F, 4G	31372_37955	2
		5A	31302_37874	0.5	5F.1	31376_37958	2
		5B	31340_37925	0.5	5G.1	31375_37956	2
		5C	31189_37796	0.5	5H	31370_37952	2
		5D	31328_37901	0.5	5I	31419_37996	0.5
		F-1B	31221_37818	2	5K	31396_37974	0.5
P	2400	4D	31223_38146	2	5L	31381_37965	2
		5E	31221_38152	2	5M	31408_37985	0.5
					5N	31432_38007	0.5
					4H	31372_38095	2
					5F.2	31376_38090	2
					5G.2	31375_38097	2
					5J	31556_38124	0.5

E – porewater composition

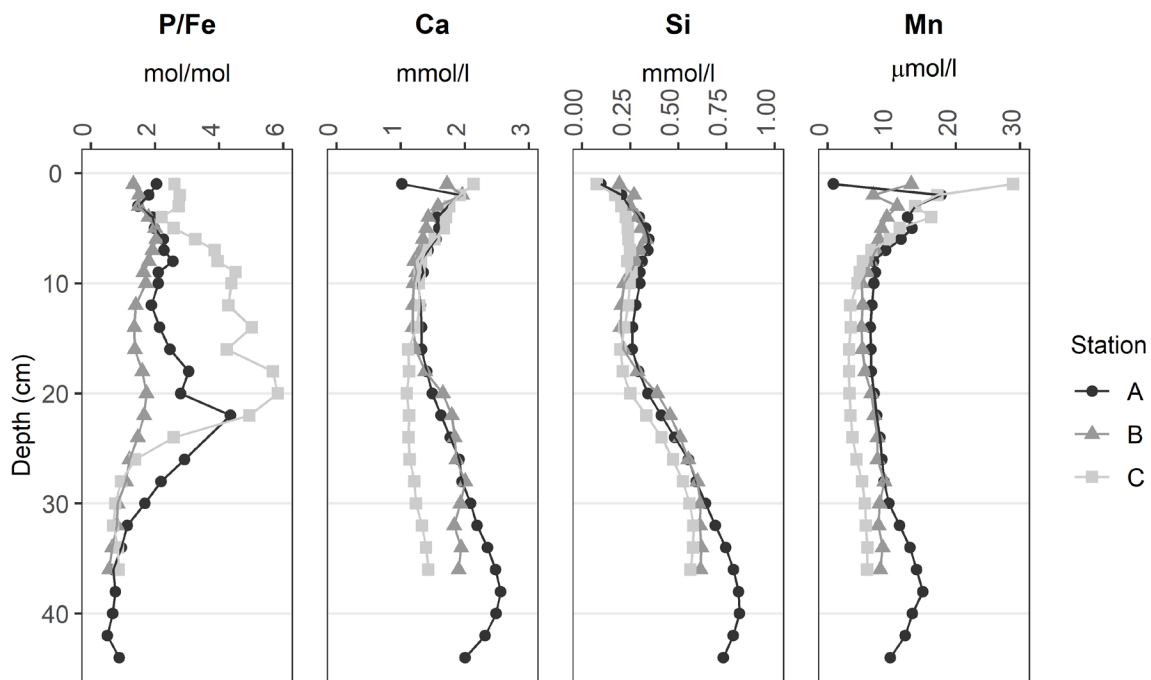


Figure E-1: Porewater composition of the cores form stations A, B and C, the same cores as were used for sequential extractions and XAS measurements. Please note the different units of the x-axes.

F – Mn distribution in the sediment solid phase

Mn and Fe are collocated in the large aggregates with comparatively low elemental densities with relative higher Mn contents at 2 cm depth (Figure F1-A) than at 40 cm depth (Figure F1-B). Correlation of the fluorescence intensities of Fe and Mn on selected areas on μ -XRF maps from each depth, further support that Fe and Mn are probably present in the same co-precipitate (Figure F-1, Figure F-2). At 2 cm depth this co-precipitate contains approximately twice as much Mn than at 40 cm depth, as is reflected in the slope of the linear fit when plotting fluorescence intensities of Fe against those of Mn (Figure F-2).

To reduce the effect of an interference of the K- α emission of Fe with the K- β emission of Mn, the μ -XRF maps shown in Figure F-1 were fitted without fixing non-linear parameters such as peak position and width (Solé et al., 2007).

For the correlation of Fe and Mn relative intensities (Figure F-2), areas on the μ -XRF maps of large aggregates were selected with low abundance of Fe hotspots reflecting iron-sulfide particles. The Fe and Mn fluorescence intensities were plotted against each other and fitted using linear regression forced through the origin.

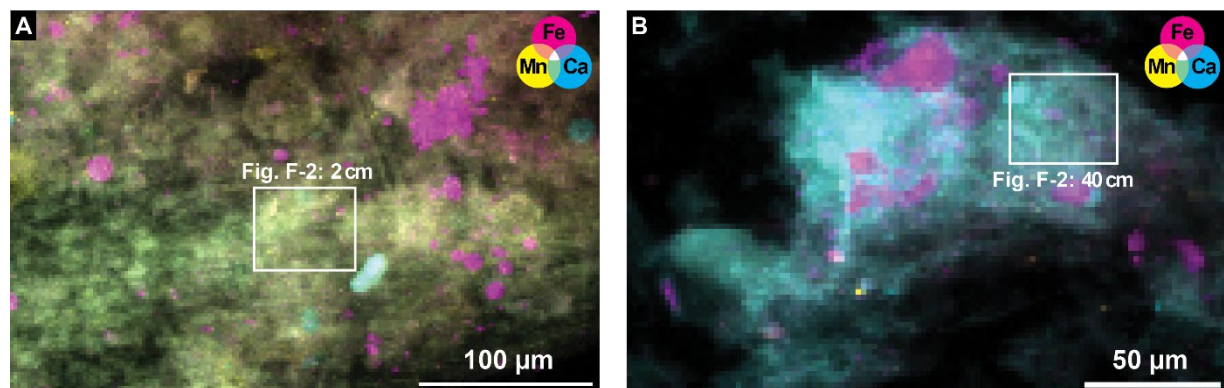


Figure F-1: μ -XRF maps showing Fe, Mn and Ca distribution collected at 7200 eV on samples from 2 cm depth (A) and 40 cm depth (B). Both maps correspond to maps shown in the main manuscript: (A) Figure 5E (measured at Fe K-edge energy) and (B) Figure 5H, and (F) Figure 5M. The identities of the maps are listed in ESI Table D1-1. The white rectangles designate the part of the map that was used for correlation of Fe and Mn shown in Figure F-2.

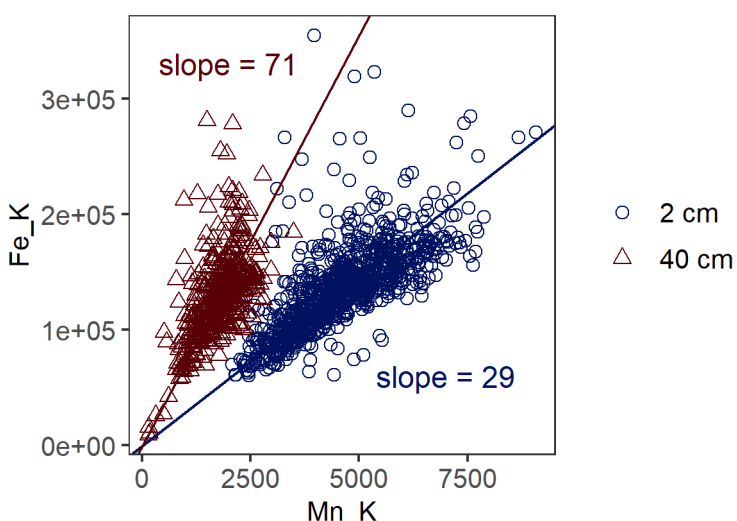


Figure F-2: Correlation of the relative intensities of the fluorescence of Fe and Mn on selected areas of two μ -XRF maps collected on samples from 2 cm (blue circles, Figure F-1 A) and 40 cm (red triangles, Figure F1-B), respectively. Linear regression fits forced through the origin are shown as lines of the respective color with the slope annotated next to the respective data points.

References

- Abrahamson, H.B., Rezvani, A.B., Brushmiller, J.G., 1994. Photochemical and spectroscopic studies of complexes, of iron (III) with citric acid and other carboxylic acids. *Inorganica Chim Acta* 226, 117–127.
- Al-Borno, A., Tomson, M.B., 1994. The temperature dependence of the solubility product constant of vivianite. *Geochim Cosmochim Acta* 58, 5373–5378.
- Bras, W., Myles, D.A.A., Felici, R., 2021. When x-rays alter the course of your experiments. *Journal of Physics: Condensed Matter* 33, 423002.
- Burton, E.D., Bush, R.T., Sullivan, L.A., Hocking, R.K., Mitchell, D.R.G., Johnston, S.G., Fitzpatrick, R.W., Raven, M., McClure, S., Jang, L.Y., 2009. Iron-Monosulfide Oxidation in Natural Sediments: Resolving Microbially Mediated S Transformations Using XANES, Electron Microscopy, and Selective Extractions. *Environ Sci Technol* 43, 3128–3134. <https://doi.org/10.1021/es8036548>
- Chen, X., Zhang, X., Wan, J., Wang, Z., Qian, Y., 2005. Selective fabrication of metastable greigite (Fe_3S_4) nanocrystallites and its magnetic properties through a simple solution-based route. *Chem Phys Lett* 403, 396–399.
- Colocho Hurtarte, L.C., Santana Amorim, H.C., Kruse, J., Criginski Cezar, J., Klysubun, W., Prietzel, J., 2020. A Novel Approach for the Quantification of Different Inorganic and Organic Phosphorus Compounds in Environmental Samples by P L2,3-Edge X-ray Absorption Near-Edge Structure (XANES) Spectroscopy. *Environ Sci Technol* 54, 2812–2820. <https://doi.org/10.1021/acs.est.9b07018>
- Colocho Hurtarte, L.C., Souza-Filho, L.F., Oliveira Santos, W., Vergütz, L., Prietzel, J., Hesterberg, D., 2019. Optimization of Data Processing Minimizes Impact of Self-Absorption on Phosphorus Speciation Results by P K-Edge XANES. *Soil Syst*. <https://doi.org/10.3390/soilsystems3030061>
- Frommer, J., Voegelin, A., Dittmar, J., Marcus, M.A., Kretzschmar, R., 2011. Biogeochemical processes and arsenic enrichment around rice roots in paddy soil: results from micro-focused X-ray spectroscopy. *Eur J Soil Sci* 62, 305–317.
- He, Z., Honeycutt, C.W., Zhang, T., Bertsch, P.M., 2006. Preparation and FT-IR characterization of metal phytate compounds. *J Environ Qual* 35, 1319–1328.
- Krizek, D.T., Bennett, J.H., Brown, J.C., Zaharieva, T., Norris, K.H., 1982. Photochemical reduction of iron. I. Light reactions. *J Plant Nutr* 5, 323–333.
- Ma, M., Overvest, P., Hijlkema, A., Mangold, S., McCammon, C., Voegelin, A., Behrends, T., 2023. Phosphate burial in aquatic sediments: Rates and mechanisms of vivianite formation from mackinawite. *Chemical Engineering Journal Advances* 16, 100565.
- Mikutta, C., Kretzschmar, R., 2011. Spectroscopic evidence for ternary complex formation between arsenate and ferric iron complexes of humic substances. *Environ Sci Technol* 45, 9550–9557.
- Münch, M.A., van Kaam, R., As, K., Peiffer, S., Heerdt, G. ter, Slomp, C.P., Behrends, T., 2023. Impact of iron addition on phosphorus dynamics in sediments of a shallow peat lake 10 years after treatment. *Water Res* 120844. <https://doi.org/10.1016/j.watres.2023.120844>
- Prietzel, J., Harrington, G., Hausler, W., Heister, K., Werner, F., Klysubun, W., 2016. Reference spectra of important adsorbed organic and inorganic phosphate binding forms for soil P speciation using synchrotron-based K-edge XANES spectroscopy. *J Synchrotron Radiat* 23, 532–544.
- Senn, A.C., Kaegi, R., Hug, S.J., Hering, J.G., Mangold, S., Voegelin, A., 2015. Composition and structure of Fe(III)-precipitates formed by Fe(II) oxidation in water at near-neutral pH: Interdependent effects of phosphate, silicate and Ca. *Geochim Cosmochim Acta* 162, 220–246. <https://doi.org/10.1016/J.GCA.2015.04.032>
- Solé, V.A., Papillon, E., Cotte, M., Walter, P., Susini, J., 2007. A multiplatform code for the analysis of energy-dispersive X-ray fluorescence spectra. *Spectrochim Acta Part B At Spectrosc* 62, 63–68.
- Terzano, R., Mimmo, T., Vekemans, B., Vincze, L., Falkenberg, G., Tomasi, N., Schnell Ramos, M., Pinton, R., Cesco, S., 2013. Iron (Fe) speciation in xylem sap by XANES at a high brilliant synchrotron X-ray source: opportunities and limitations. *Anal Bioanal Chem* 405, 5411–5419.

Wielinski, J., Jimenez-Martinez, J., Göttlicher, J., Steininger, R., Mangold, S., Hug, S.J., Berg, M., Voegelin, A., 2022. Spatiotemporal Mineral Phase Evolution and Arsenic Retention in Microfluidic Models of Zervalent Iron-Based Water Treatment. *Environ Sci Technol* 56, 13696–13708. <https://doi.org/10.1021/acs.est.2c02189>

Wolthers, M., Van Der Gaast, S.J., Rickard, D., 2003. The structure of disordered mackinawite. *American Mineralogist* 88, 2007–2015. <https://doi.org/doi:10.2138/am-2003-11-1245>